bond. Both mechanisms generate *tert*-butylhydroaminoxyl radical.

Acknowledgment. The National Biomedical Center for Spin Trapping and Free Radicals is supported by the Biomedical Research Technology Program of the National Center for Research Resources in National Institutes of Health Grant No. RR05517-01A1. Grateful acknowledgement is hereby made.

Registry No. 1, 55482-05-8; **2**, 22665-15-2; **2-*N*-*d***, 136587-04-7; D_2, 7782-39-0.

Applications of Real-Time FTIR Spectroscopy to the Elucidation of Complex Electroorganic Pathways: Electrooxidation of Ethylene Glycol on Gold, Platinum, and Nickel in Alkaline Solution

Si-Chung Chang,† Yeunghaw Ho, and Michael J. Weaver*

Contribution from the Department of Chemistry, Purdue University, West Lafayette, Indiana 47907. *Received June 19, 1991*

Abstract: The electrooxidation pathways of ethylene glycol in alkaline aqueous solution on gold, platinum, and nickel electrodes are explored by means of real-time FTIR spectroscopy in conjunction with cyclic voltammetry. The former enables a quantitative assay of specific intermediates and products formed during the reaction evolution. The electrooxidation on gold features the successive formation of partially oxidized C_2 solution species en route to oxalate and carbonate production. The latter species is produced predominantly via the formation of the dialdehyde, glyoxal, based on comparisons with electrooxidative spectral sequences for candidate intermediate species. In contrast, ethylene glycol electrooxidation on platinum exhibits markedly different kinetics and product distributions to those for the partially oxidized C_2 species, inferring that at least carbonate production from ethylene glycol occurs largely through sequences of chemisorbed, rather than solution-phase, intermediates. Electrooxidation of ethylene glycol and higher polyols on nickel display a remarkably selective production of formate. This efficient oxidative C–C bond cleavage on nickel is displayed in somewhat different fashion for partially oxidized C_2 reactants in that carbonate is predominantly formed. Some possible surface chemical factors responsible for these striking mechanistic differences are discussed.

Introduction

While often overlooked by chemists, electrochemistry can provide a highly controllable as well as flexible means with which to undertake redox-induced transformations of organic molecules. A limitation of purely electrochemical measurements, however, is that little specific information can be discerned regarding the identity of reaction intermediates and hence detailed reaction pathways. This difficulty can be circumvented in part by combining electrochemical methods with other techniques, such as optical and mass spectroscopies and chromatography. These additional techniques are often limited to postelectrolytic analysis, however, thereby being restricted largely to the identification of final reaction products.

The use of thin-layer electrochemistry combined with Fourier-transform infrared spectroscopy provides a relatively straightforward, yet powerful, means of providing real-time (ca. 1-s time scale) vibrational characterization of the solution as well as the surface electrode composition as such electrochemical processes proceed.[1-5] Given the well-known suitability of infrared spectroscopy for functional-group characterization, this tactic should constitute a quantitative means of assessing the kinetics of specific molecular transformations, thus providing a valuable adjunct to the overall reaction kinetics obtained from simultaneously acquired electrochemical data.[3a,d]

A simple variant of such real-time spectroelectrochemical measurements, utilized here, involves obtaining sequences of FTIR spectra during a single potential sweep or step. Subtraction of appropriate spectra is undertaken so to remove solvent and other interferences, exposing the potential-dependent components associated chiefly with the desired redox-induced changes in thin-layer solute composition. We have dubbed this type of procedure "single potential alteration infrared spectroscopy" (SPAIRS) to distinguish it from other potential-difference procedures that feature repeated modulations.[2] Within limits, such vibrational spectral information should become increasingly valuable as the complexity of the reaction pathway becomes greater. A number of such studies for both organic and inorganic redox systems have appeared recently;[1-5] however, the virtues of the approach from an organic mechanistic standpoint have yet to be fully exploited.

Outlined herein is a straightforward, yet we believe insightful, examination of electrooxidation pathways discerned in this fashion for ethylene glycol and related polyhydric alcohols in alkaline aqueous solution at polycrystalline gold, platinum, and nickel surfaces. Ethylene glycol is of interest not only as a possible candidate for fuel-cell development but also in view of extensive previous electrochemical examinations of its oxidation on platinum[2] and gold.[3] In spite of these activities, the oxidation mechanisms are poorly understood, in part with regard to the role of the several possible partly oxidized (aldehyde, carboxylate) species in the

† Present address: Dow Chemical Co., Midland, MI 48667.

(1) For a recent review, see: Christensen, P. A.; Hamnett, A. In *Comprehensive Chemical Kinetics*, Compton, R. G., Hamnett, A., Eds.; Elsevier: Amsterdam, 1989; Vol. 29, Chapter 2.

(2) Corrigan, D. S.; Leung, L.-W. H.; Weaver, M. J. *Anal. Chem.* **1987**, *59*, 2252.

(3) Recent examples from our laboratory for electroorganic processes: (a) Leung, L.-W. H.; Weaver, M. J. *J. Phys. Chem.* **1988**, *92*, 4019. (b) Leung, L.-W. H.; Chang, S.-C.; Weaver, M. J. *J. Electroanal. Chem.* **1989**, *266*, 317. (c) Leung, L.-W. H.; Weaver, M. J. *J. Phys. Chem.* **1989**, *93*, 7218. (d) Leung, L.-W. H.; Weaver, M. J. *Langmuir* **1990**, *6*, 323. (e) Chang, S.-C.; Leung, L.-W.; Weaver, M. J. *J. Phys. Chem.* **1990**, *94*, 6013.

(4) (a) Nishimura, K.; Kunimatsu, K.; Machida, K. I.; Enyo, M. *J. Electroanal. Chem.* **1989**, *260*, 181. (b) Sun, S. G.; Yang, D.-F.; Tian, Z.-W. *J. Electroanal. Chem.* **1990**, *289*, 177.

(5) For example, see: (a) Bullock, J. P.; Palazotto, M. C.; Mann, K. R. *Inorg. Chem.* **1991**, *30*, 1284. (b) Lewis, G. J.; Roth, J. D.; Safford, L. K.; Gao, X.; Chang, S.-C.; Dahl, L. F.; Weaver, M. J. *J. Am. Chem. Soc.* **1990**, *112*, 2831.

0002-7863/91/1513-9506$02.50/0

overall reaction.[6,7] Infrared spectroscopy has recently been harnessed to identify carbon monoxide and other species formed from ethylene glycol on platinum[3d,6c] and to identify some reaction products in acidic and basic media.[7a,8] The cleavage of the C–C bond to yield exhaustive electrooxidation of ethylene glycol in acidic and alkaline media has been noted on platinum[3a,d,8] and in alkaline solutions on gold.[7a] Despite the widespread interest shown in the electrocatalytic properties of oxidized nickel surfaces in base,[9] little mechanistic information exists for ethylene glycol oxidation in this environment. A particular mechanistic tactic exploited here is to examine by means of real-time FTIR spectroelectrochemistry the electrooxidation characteristics of various candidate species expected to be intermediates for ethylene glycol oxidation. These findings lead to some appreciation of the sensitivity of the electrooxidation pathways to the metal catalyst and the underlying molecular factors involved.

Experimental Section

Most experimental details concerning the infrared instrumentation and procedures are given in refs 2, 3a, and 10. A Bruker-IBM IR 98-4A Fourier transform instrument was employed, with a Globar light source and an MCT narrow-band detector (Infrared Associates). The spectral resolution was 4 cm^{-1}. The electrochemical infrared measurements were performed by pushing the electrode up to a CaF_2 optical window, so to form a thin (ca. 5 μm) solution layer. The polycrystalline gold surface was pretreated immediately prior to use by mechanical polishing, dipping in hot chromic acid, followed by rinsing, and potential cycling in aqueous 0.5 M KOH (ultra pure, Alfa) at 0.1 V s^{-1} between −1.0 and 0.6 V vs SCE for 10 min. The polycrystalline nickel surface was first polished with fine alumina down to 0.05 μm, then thoroughly rinsed with ultrapure water, and rapidly transferred to the infrared cell. Bulk-solution infrared spectra were measured with a transmittance IR cell (0.0125-mm path length) with either CaF_2 or ZnSe windows.

Ethylene glycol and glyoxal were obtained from Aldrich and glycolate and glyoxylate from Strem Chemical and Fluka, respectively. All chemicals were used as received. Water was purified by means of a "Milli-Q" system (Millipore). Electrode potentials are quoted with respect to the saturated calomel electrode (SCE), and all measurements were performed at 23 ± 1 °C.

Results and Discussion

Typical anodic–cathodic cyclic voltammograms obtained at 50 mV s^{-1} for 50 mM ethylene glycol on gold, platinum, and nickel electrodes in 0.5 M KOH, sweeping initially positive from −0.9 V vs SCE, are shown as solid traces in Figure 1A–C, respectively. The dashed curves are the corresponding voltammograms recorded in the supporting electrolyte alone. These voltammetric features for ethylene glycol electrooxidation were reproducible upon repetitive potential cycling. Similar features were obtained if slower voltammetric scan rates, down to 1 mV s^{-1}, were used along with the thin-layer configuration required for simultaneous FTIR measurements. Figure 1A,B shows that the initiation of ethylene glycol electrooxidation on gold and platinum occurs well before the commencement of anodic oxide formation (compare solid, dotted traces). On nickel, the onset of ethylene glycol electrooxidation corresponds closely with the potential of the surface redox wave associated with the formation of "NiOOH" from $Ni(OH)_2$ (vide infra).[9,10,12]

Scheme I

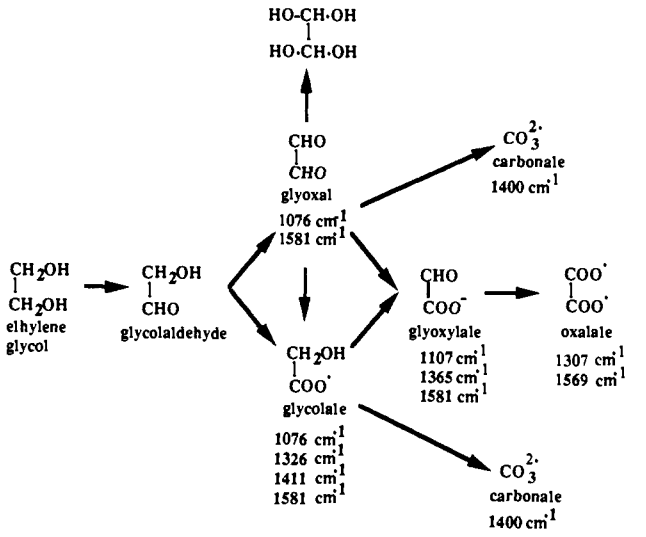

Table I. Frequencies (cm^{-1}) and Integrated Absorptivities (M^{-1} cm^{-1}) of Major Infrared Bands for Various Candidate Species Formed in Electrooxidations, as Determined by Solution Transmittance Measurements

molecules	asy(COO^-)[a,c] (cm^{-1})	sym(COO^-)[b] (cm^{-1})	other bands (cm^{-1})
carbonate			1390–1410 (8.4×10^4)
formate	1581 (3.3×10^4)[b]	1350 1381 (6.4×10^3)	
acetate	1550 (1.7×10^4)	1411 (8.9×10^3)	
glyoxal	1581		1076 (3.2×10^3)
glycolate	1581	1326 (4.5×10^3) 1411 (6.5×10^3)	1076 (5.2×10^3)
glyoxylate	1581	1365 (6.5×10^3)	1107 (8.8×10^3)
oxalate	1569 (1.4×10^4)	1307 (8.0×10^3)	

[a] Frequencies of asymmetric COO or C–O stretches. [b] Frequencies of symmetric COO stretches. [c] Integrated absorptivities (M^{-1} cm^{-1}) of infrared bands given in parentheses underneath corresponding frequency value.

Of central concern here is the identification of the various species formed in such electrochemical experiments; the rather featureless voltammograms in Figure 1A–C belie the rich sequences of molecular transformations that are responsible for the observed anodic currents. The balance of this paper focusses chiefly on the extraction of such information for ethylene glycol electrooxidation from SPAIR spectra. A likely reaction sequence (cf. ref 7a) is shown as Scheme I, involving stepwise sequential oxidation of the alcohol moieties to aldehydes and carboxylates, maintaining the C_2 difunctionality. Scission of the C–C bond at any stage can also be envisaged, leading ultimately to the formation of CO_2, and hence to carbonate (CO_3^{2-}) in the alkaline solutions used here.

Several of these potential reaction intermediates exhibit clearly discernable and diagnostic spectral features in the mid-infrared region. Some major band frequencies are included in Scheme I and in Table I. The latter includes integrated molar absorptivities, ϵ_b (given in parentheses), obtained along with the peak frequencies, ν^p, from infrared bulk transmittance spectra in aqueous 0.1 M KOH. Contained along with the C_2 compounds

(6) Kazarinov, V. E.; Vassiliev, Y. B.; Andreev, V. N.; Horanyi, G. *J. Electroanal. Chem.* **1983**, *147*, 247. (b) Hauffe, W.; Heitbaum, J. *Electrochim. Acta* **1978**, *23*, 299. (c) Hahn, F.; Beden, B.; Kadirgan, F.; Lamy, C. *J. Electroanal. Chem.* **1987**, *216*, 169.

(7) (a) Kadirgan, F.; Charbonnier, E. B.; Lamy, C.; Beden, B. *J. Electroanal. Chem.* **1990**, *286*, 41; (b) Lamy, C. *Electrochim. Acta* **1984**, *29*, 1581; (c) Beden, B.; Cetin, L.; Kahyaoglu, A.; Takky, D.; Lamy, C. *J. Catal.* **1987**, *104*, 37. (d) Hauffe, W.; Heitbaum, J. *Ber. Bunsenges. Phys. Chem.* **1978**, *82*, 487.

(8) Christensen, P. A.; Hamnett, A. *J. Electroanal. Chem.* **1989**, *260*, 347.

(9) For recent reviews, see: Schafer, H.-J. *Topics in Current Chemistry*; Steckhan, E., Ed.; 1987; Vol. 142, p 101. (b) McBreen, J. *Modern Aspects of Electrochemistry*; White, R. E., Bockris, J. O'M.; Conway, B. E. 1990; Vol. 21, Chapter 2.

(10) (a) Corrigan, D. S.; Weaver, M. J. *J. Phys. Chem.* **1986**, *90*, 5300. (b) Corrigan, D. S.; Weaver, M. J. *J. Electroanal. Chem.* **1988**, *241*, 143.

(11) For example: Fleischmann, M.; Korinek, K.; Pletcher, D. *J. Chem. Soc., Perkin Trans. II* **1972**, 1396.

(12) Desilvestro, J.; Corrigan, D. A.; Weaver, M. J. *J. Electrochem. Soc.* **1988**, *135*, 885.

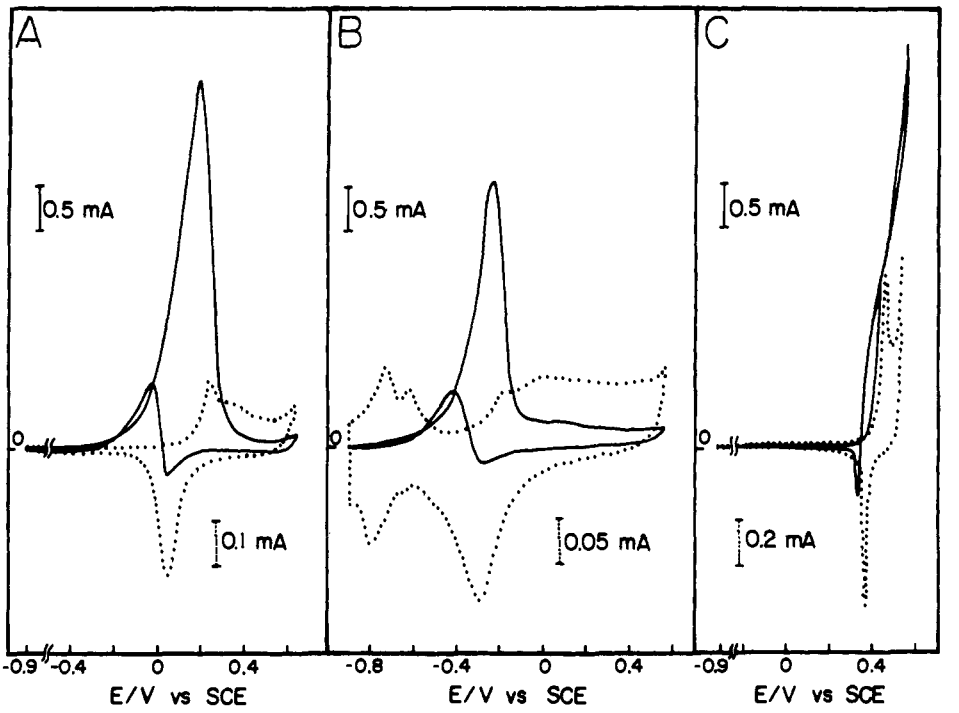

Figure 1. Cyclic voltammograms obtained at 50 mV s^{-1} for the electrooxidation of 50 mM ethylene glycol on (A) gold, (B) platinum, and (C) nickel electrodes in 0.5 M KOH (solid traces) (electrode area = 0.7 cm^2 for platinum, gold, and nickel electrodes). Dotted traces are the corresponding voltammograms in 0.5 M KOH alone.

in Table I are corresponding ν^p and ϵ_b data for other possible product species: formate, acetate, and carbonate. The assignment of asymmetric and symmetric carboxylate vibrations (ν_{asy} and ν_{sym}) given in Table I is inferred from that for acetate and related species.[13] Glycolaldehyde ($OCH{\cdot}CH_2OH$) is not included in Table I. This compound exhibits relatively featureless spectra in neutral aqueous media, due to dimerization and other equilibria;[14] further complications ensue in alkaline solution as gleaned from a yellow coloration appearing within 1–2 min. The characterization of glyoxal ($OHC{\cdot}CHO$) also suffers complications arising from hydrolysis[15] and the formation of glycolate by the Canizzaro reaction.[16] However, evidence that the glyoxal–glycolate transformation is incomplete (≲30% conversion) in 0.5 M KOH on the relevant time scale here (≲30 min) was obtained from the observation of significantly different transmittance spectra for these two species (Table I) along with differing SPAIR spectra for their electrooxidation on gold (vide infra).

Electrooxidation on Gold. A typical sequence of SPAIR spectra in the 1000–2500-cm^{-1} region obtained during the voltammetric oxidation of 50 mM ethylene glycol in 0.5 M KOH on gold is shown in Figure 2A. The voltammetric sweep rate is 2 mV s^{-1}, positive-going from −0.5 to 0.6 V. Each spectrum shown in Figure 2A involved acquiring 50 interferometer scans (consuming ca. 30 s), subtracted from which was a spectrum recorded at the initial potential so to minimize solvent spectral interferences.[3] Only selected members of the sequence are shown for clarity; the potentials indicated alongside each spectrum are the average values during the data acquisition. (The concentrated, 0.5 M, hydroxide electrolyte was chosen so to buffer the solution against pH changes resulting from the protons released into the thin layer as products of the organic electrooxidations.)

Several spectral features in Figure 2A provide information on the species formed during ethylene glycol electrooxidation. In the "relative transmittance" format shown, positive- and negative-going bands arise from species consumed and produced, respectively, in the oxidation process. Of the former, the chief bands for ethylene glycol, at ca. 1025 and 1050 cm^{-1} (C–O stretching), are located at frequencies below those characterizing the various oxidation products, so that these positive-going features seen in

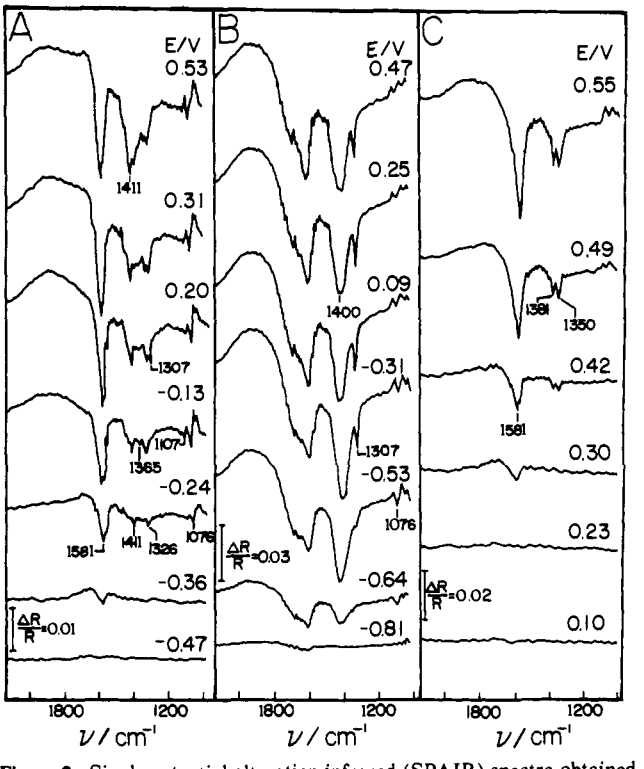

Figure 2. Single potential alteration infrared (SPAIR) spectra obtained during the voltammetric oxidation of 50 mM ethylene glycol on (A) gold, (B) platinum, and (C) nickel electrodes in 0.5 M KOH. Potential sweep rate was 2 mV s^{-1}, positive going from −0.5, −0.85, and 0.0 V vs SCE for (A), (B), and (C), respectively. Each spectrum, displayed as relative reflectance ($\Delta R/R$), was acquired from 50 interferometer scans at the average potentials indicated, ratioed to the corresponding spectrum obtained at the initial potential.

(13) Silverstein, R. M.; Bassler, R. C.; Morrill, T. C. In *Spectrometric Identification of Organic Compounds*; Wiley: New York, 1981; Chapter 3.
(14) (a) Guthrie, J. P. *Can. J. Chem.* **1975**, *53*, 898. (b) Glushonok, G. K.; Petryaev, E. P.; Shadyro, O. I. *Russ. J. Phys. Chem.* **1984**, *58*, 57–59.
(15) (a) Whipple, E. B. *J. Am. Chem. Soc.* **1970**, *92*, 7183. (b) Fratzke, A. R.; Reilly, P. J. *Int. J. Chem. Kinet.* **1986**, *18*, 775.
(16) (a) Salomaa, P. *Acta Chem. Scand.* **1956**, *10*, 311. (b) Fratzke, R.; Reilly, P. J. *Int. J. Chem. Kinet.* **1986**, *18*, 757.

Figure 2A,B do not interfere significantly with the negative-going bands for the latter.

Following the onset of anodic current at ca. −0.25 V on gold, several negative-going features are observed in Figure 2A. The bands seen at 1326 and 1411 cm^{-1} (ν_{sym} pair) are diagnostic of the formation of glycolate, $HOCH_2$–COO^- (Table I). The additional negative-going bands seen at 1581 and 1076 cm^{-1} also appear in the solution transmittance spectrum for glyoxal, OHC·CHO (Table I). The glycolate 1326/1411 cm^{-1} features grow in intensity as the potential becomes more positive on gold, indicating that this species is present increasingly during the excursion through the anodic voltammetric wave (Figure 1A). At potentials around −0.1 V, an additional pair of bands at 1365 and 1107 cm^{-1} are observed (Figure 2A); these features signal the production of glyoxylate, OHC·COO^- (Table I). These bands diminish in intensity by 0.1–0.2 V, and a new feature at 1307 cm^{-1} grows in at potentials positive of 0 V. The latter is diagnostic of the production of oxalate (Table I). At higher potentials, beyond ca. 0.4 V, a broad negative-going feature at ca 1400 cm^{-1} becomes increasingly discernable, forming a "hollow" within which the sharper bands at comparable frequencies are contained (Figure 2A). This band is indicative of the formation of the exhaustive electrooxidation product, carbonate (Table I).

These results can be interpreted simply in terms of the reaction sequence in Scheme I. The major issue at hand is elucidating the possible roles of the intermediates shown in Scheme I and establishing the likely routes by which the overall products observed in the SPAIR spectra are produced. A valuable tactic for this purpose involves examining by means of SPAIRS the voltammetric oxidation of the various C_2 candidate species anticipated to constitute solution-phase intermediates for ethylene glycol electrooxidation (Scheme I). Of the five possibilities, as noted above, glycolaldehyde cannot be examined in this manner due to self-polymerization that occurs in alkaline aqueous solution.[14b] Oxalate does not undergo any significant electrooxidation on either gold or platinum in 0.5 M KOH, at least up to 0.6 V. The remaining three candidate species, glycolate, glyoxal, and glyoxylate, readily undergo electrooxidation; SPAIR spectra obtained during their voltammetric oxidation at gold in 0.5 M KOH are shown in Figure 3A–C, respectively. The experimental conditions in Figure 3 are identical with those in Figure 2.

Two primary negative-going bands are apparent in Figure 3A–C; as before, the features at ca. 1400 and 1307 cm^{-1} are diagnostic of the formation of carbonate and oxalate, respectively. (The third feature, observed around 1580 cm^{-1}, is less useful diagnostically; it probably contains components arising from the consumption of the reactant as well as products, since most C_2 intermediates exhibit a band at this frequency, Table I.) Comparison of the intensities of the 1400- and 1307-cm^{-1} features in Figure 3A–C provides useful information on the differing product distributions for these reactions. Most noticeably, glyoxylate electrooxidation yields only oxalate, no discernable carbonate feature being obtained (Figure 3C). Glycolate and glyoxal, on the other hand, oxidize to yield both oxalate and carbonate as discerned from the parallel appearance of the 1307- and 1400-cm^{-1} features in Figure 3A,B. As for the electrooxidation of ethylene glycol, oxalate appears initially at lower potentials than does carbonate.

The electrooxidations of glycolate and glyoxal show two significant differences. The extent of reaction is smaller for the former species, as discerned from both the SPAIR spectra and the corresponding voltammetric currents. In addition, glyoxal yields substantially more carbonate, and less oxalate, than is the case for glycolate. For example, the ratio of carbonate to oxalate formed at 0.6 V is ca. 0.2 and 1.5 for glycolate and glyoxal electrooxidation, respectively, as deduced from the spectral intensities in Figure 3A,B along with the band absorptivities in Table I.

Intercomparison of these findings with the corresponding SPAIR spectra for ethylene glycol electrooxidation (Figure 2) indicates that glyoxal probably constitutes the major solution intermediate. This deduction can be made by noting that the form

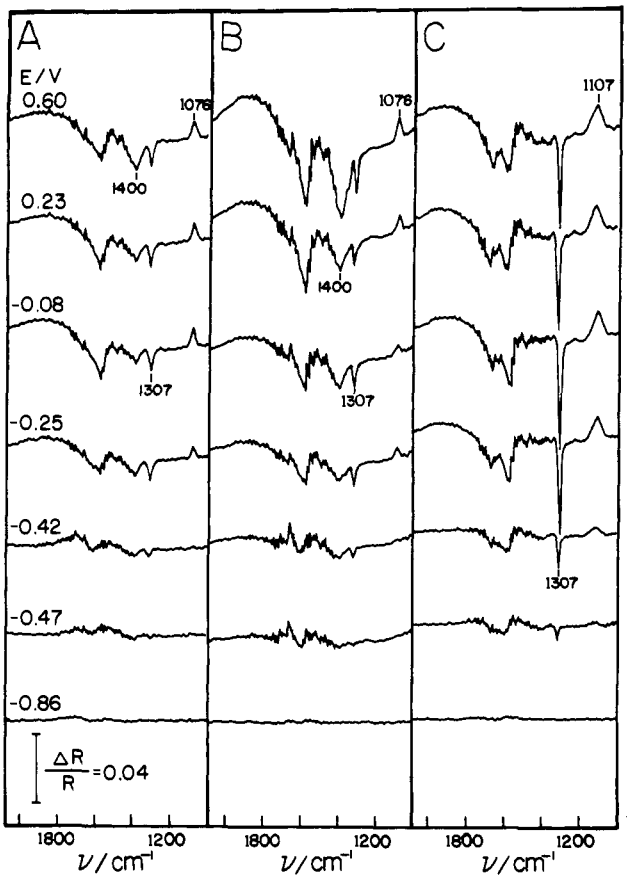

Figure 3. SPAIR spectra obtained during the voltammetric oxidation of (A) 50 mM glycolate, (B) 50 mM glyoxal, and (C) 50 mM glyoxylate in 0.5 M KOH on gold. Potential sweep rate was 2 mV s^{-1}, positive going from −0.9 V. Other details are as in Figure 2.

of the glyoxal SPAIR spectra (Figure 3B), at least with regard to the carbonate/oxalate ratios, are markedly closer to matching those observed for the ethylene glycol spectra (Figure 2A). This observation does not necessarily deny a significant role to glycolate as a reaction intermediate, especially since partial (albeit incomplete) interconversion of glycolate and glyoxal can occur on the experimental time scale (vide supra). Nonetheless, the evidence indicates that the preferred reaction pathway involves the intermediate formation of the symmetric dialdehyde glyoxal, rather than the unsymmetric partially oxidized species glycolate. The observation that the further oxidized form of glycolate, glyoxylate, does not yield carbonate as a reaction product diminishes the likely importance of the lower parallel pathway in Scheme I in the overall electrooxidation kinetics at high potentials where carbonate is primarily formed. Nonetheless, the observation from the SPAIR spectra that glyoxylate and glycolate are also formed at lower potentials during ethylene glycol electrooxidation (Figure 2, vide supra) indicates that these species as well as glyoxal are involved significantly in the overall reaction. Consistent with this sequential potential-dependent formation of solution-phase intermediates is the observation that the onset of voltammetric current for ethylene glycol electrooxidation on gold (ca. −0.25 V, Figure 1A) occurs at significantly lower potentials than for glyoxal (ca. 0 V).

It is appropriate to compare briefly these mechanistic features with those deduced previously for the same reaction by Kadirgan et al.[7a] using bulk electrolysis followed by liquid chromatography and infrared transmittance measurements. In contrast to the present findings, these authors concluded that oxalate along with formate constitute the primary end products, being formed via glycolate. The present SPAIR spectra, however, provide no evidence for formate production. One limitation of the study of Kadirgan et al. is that they were apparently unable to analyze for carbonate; according to the present measurements this species constitutes the major reaction product, at least at high potentials.

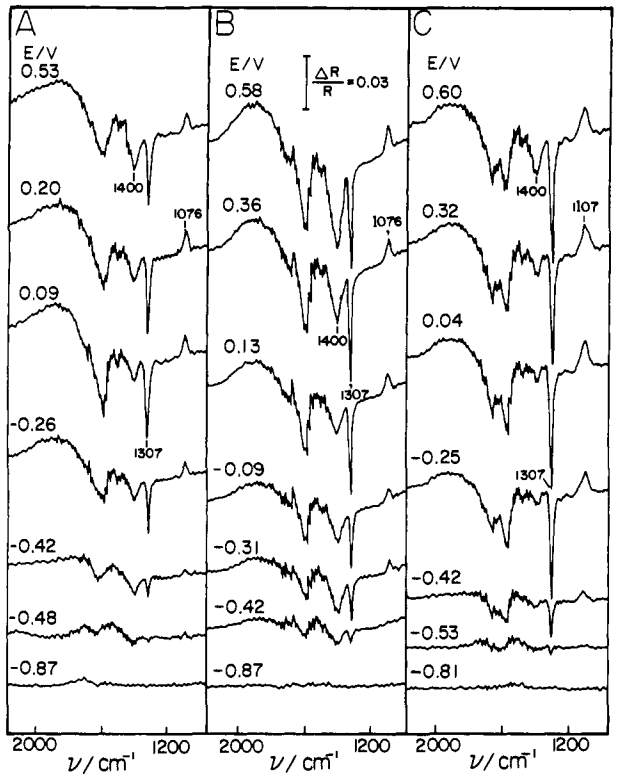

Figure 4. SPAIR spectra obtained during the voltammetric oxidation of (A) 50 mM glycolate, (B) 50 mM glyoxal, and (C) 50 mM glyoxylate in 0.5 M KOH on platinum. Potential sweep rate was 2 mV s^{-1}, positive going from −0.9 V. Other details are as in Figure 2.

An obvious advantage of the SPAIRS procedure employed here is that it provides a real-time in situ analysis of the product distribution under bona fide reaction conditions.

Electrooxidation on Platinum. A similar series of voltammetric SPAIRS measurements was also undertaken on platinum in 0.5 M KOH. A typical SPAIR spectral sequence obtained for the electrooxidation of 50 mM ethylene glycol on platinum is shown in Figure 2B. This series was obtained in the same manner as that on gold (Figure 2A) but by sweeping the potential instead from −0.9 V. In contrast to gold, the negative-going 1400-cm^{-1} feature due to carbonate formation appears at relatively negative potentials, ca. −0.6 V, close to the onset of anodic current. The 1307-cm^{-1} band diagnostic of oxalate production also appears clearly by ca. −0.4 V (Figure 2B). The other negative-going band, at 1550–1580 cm^{-1}, is associated in part with oxalate formation. This feature could also arise from partly oxidized C_2 species as well as from formate ($HCOO^-$) formed by C–C bond scission. At least the dominant intermediate production of glycolate and glyoxylate, observed for gold, does not occur on platinum as evidenced by the absence of the diagnostic sharp bands characterizing the former species in the 1320–1370-cm^{-1} region. The weak feature at 1076 cm^{-1} seen at more negative potentials on platinum (Figure 2B) is nonetheless consistent with some intermediate production of glycolate and/or glyoxal. A similar finding was reported in ref 8.

As for electrooxidation on gold, it is instructive to compare these SPAIR spectra for ethylene glycol on platinum with corresponding data obtained for candidate reaction intermediates. Figure 4A–C shows such data for the electrooxidation of 50 mM glycolate, glyoxal, and glyoxylate, respectively, in 0.5 M KOH (cf. Figure 3A–C on gold). The spectra in Figure 4A–C display uniformly different potential-dependent features than are seen for ethylene glycol electrooxidation on platinum (Figure 2B). The latter show that substantially greater quantities of carbonate are formed, and at lower potentials, from ethylene glycol than is the case for any of the three candidate intermediate species, glycolate, glyoxal, and glyoxylate. Additionally, significantly more oxalate is produced from these latter three species than from ethylene glycol.

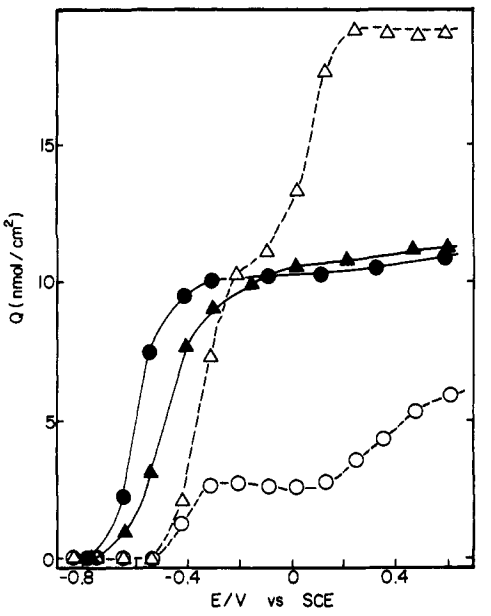

Figure 5. Plots of quantity, Q, of carbonate (triangles) and oxalate (circles) formed as a function of electrode potential during a 2 mV s^{-1} voltammetric oxidation of 50 mM ethylene glycol (filled symbols, solid traces) and glyoxal (open symbols, dashed traces), respectively, on platinum. Data were extracted from the SPAIR spectra as outlined in the text.

These differences are displayed in quantitative fashion in Figure 5, in the form of plots of the quantity (nmol cm^{-2}) of carbonate, $Q(CO_3^{2-})$ (circles), and oxalate, Q(Ox) (triangles), formed as a function of electrode potential from either ethylene glycol (filled symbols, solid lines) or glyoxal (open symbols, dashed lines) on platinum. These plots were extracted from the integrated absorbances of the 1400-cm^{-1} carbonate and 1307-cm^{-1} oxalate bands in SPAIR spectra as in Figures 2B and 4B, along with the corresponding absoptivities given in Table I. (See ref 3 for further procedural details). Note that glyoxal forms substantially (3–5 times) more oxalate than carbonate at a given electrode potential, whereas ethylene glycol yields comparable amounts of oxalate and carbonate, the latter species being formed initially. Even more marked differences are seen in corresponding comparisons between ethylene glycol and either glycolate or glyoxylate, in that the latter two species form much larger amounts of oxalate relative to carbonate (this point can readily be discerned from the spectra in Figure 4).

Mechanistic Comparisons between Gold and Platinum. In contrast to the case of gold discussed above, therefore, none of the intermediate C_2 species in Scheme I can account for the high proportion of carbonate produced from ethylene glycol electrooxidation, especially at lower potentials. Consequently, the production of carbonate from ethylene glycol is unlikely to occur via the formation of such intermediate *solution-phase* species on platinum, as is the case on gold. This finding strongly suggests that carbonate formation on platinum takes place by means of a multistep process involving intermediate (possibly short-lived) *surface*, rather than longer lived solution, species. It is reasonable to assert that the C–C bond cleavage necessary to form CO_2 (and hence carbonate in alkaline media) from ethylene glycol occurs within the adsorbed state prior to, or at least concurrent with, the necessary oxygen/proton-transfer steps. A partially oxidized species, such as glyoxal or glycolate, may be formed on the surface prior to C–C bond scission. However, desorption to form solution-phase glyoxal would not provide an effective catalytic pathway, at least at low potentials, since glyoxal is unreactive with respect to carbonate formation on platinum under these conditions.

These findings provide straightforward evidence of a major difference in catalytic action of gold versus platinum toward the exhaustive electrooxidation of ethylene glycol. While the former surface is capable of yielding carbonate, this appears to occur in a series of steps, at least some involving long-lived solution in-

termediates. Platinum, on the other hand, can effect the ten-electron oxidation necessary to convert ethylene glycol to carbonate in an inherently concerted interfacial step or series of steps. The necessary ability of platinum to dissociatively chemisorb organic reactants such as alcohols, including ethylene glycol,[6c] is well-known in electrochemical as well as gas-phase environments.[17]

It is also interesting to compare the potential regions where carbonate formation from ethylene glycol commences in relation to the onset of surface oxidation as gleaned from the voltammograms in 0.5 M KOH alone (dotted traces, Figure 1A,B). Figure 2A shows that carbonate production on gold is initiated only at potentials beyond ca. 0.4 V, well into the anodic oxide region which commences at 0.2 V (Figure 1A). This finding suggests that the C–C bond cleavage and attendant oxygen transfer involves the surface oxide film. In contrast, as noted above, carbonate production on platinum starts at potentials, ca. −0.6 V, markedly below the onset of oxide formation, at −0.2 V (Figure 1B). Consequently, then, the oxygen-transfer agent on platinum under these conditions appears to be adsorbed water or hydroxyl species.

Electrooxidation on Nickel: Ethylene Glycol and Higher Polyols. Having uncovered major mechanistic differences between gold and platinum in the exhaustive electrooxidation of ethylene glycol, it is of interest to examine the reaction pathways on a distinctly different type of metal electrocatalyst, nickel. A typical sequence of SPAIR spectra for the voltammetric oxidation of ethylene glycol in 0.5 M KOH on nickel is shown in Figure 2C. Aside from the initial potential, 0 V, the conditions used in Figure 2C are identical to those for the corresponding spectra on gold and platinum shown in Figure 2A,B, respectively. Inspection of Figure 2C indicates the occurrence of a markedly different electrooxidation pathway on nickel as compared with either gold or platinum. At potentials above 0.35 V on the first surface, three bands centered at 1350, 1381, and 1581 cm^{-1} appear in concert (Figure 2C). These three bands together constitute a clear fingerprint of the production of formate. The 1350- and 1381-cm^{-1} features are assigned to O–C–O symmetric stretching vibrations and the 1581-cm^{-1} band to the corresponding asymmetric stretch[13] (Table I). Examination of the cyclic voltammogram for ethylene glycol electrooxidation on nickel (Figure 1C) shows that the reaction, producing formate, is initiated sharply at a potential, ca. 0.4 V, corresponding to the reversible $Ni(OH)_2$/"NiOOH" couple.[9] The SPAIRS results indicate clearly that while the nickel surface has the ability to cleave the C–C bond of ethylene glycol as for platinum and gold, the primary oxidation product is quite different.

As before, it is instructive to examine the corresponding electrooxidation pathways for the candidate intermediate species glycolate, glyoxal, and glyoxylate in comparison with ethylene glycol. Typical SPAIR spectra for these three reactants on nickel are displayed in Figure 6A–C (cf. Figures 3A–C and 4A–C on gold and platinum). These spectra display markedly different features to those for ethylene glycol electrooxidation on nickel (Figure 2C). Glycolate, glyoxal, and glyoxylate each yield predominantly carbonate, together with a smaller amount of oxalate (as evidenced by the weak 1307-cm^{-1} band). The appearance of the 1581-cm^{-1} band during glyoxylate oxidation (Figure 6C) may indicate the production of some formate in this case, although the absence of the sharp 1350/1381-cm^{-1} doublet (expected to appear as shoulders on the broad carbonate band at 1400 cm^{-1}) suggests otherwise. Similarly to platinum, then, the electrooxidation of ethylene glycol on nickel is unlikely to proceed via these solution-phase intermediates. Furthermore, the "clean" cleavage of the C–C linkage to yield solely formate is only seen for the vicinal diol, ethylene glycol. Reaction of partially oxidized species containing aldehyde and/or carboxylate functional groups yields only incomplete C–C bond scission.

Not surprisingly on the above basis, formate does not display any electroactivity on nickel in 0.5 M KOH, up to 0.6 V. The same finding applies to gold. On platinum in 0.5 M KOH, however, formate undergoes facile electrooxidation, starting at

(17) Parsons, R.; VanderNoot, T. *J. Electroanal. Chem.* **1988**, *257*, 9.

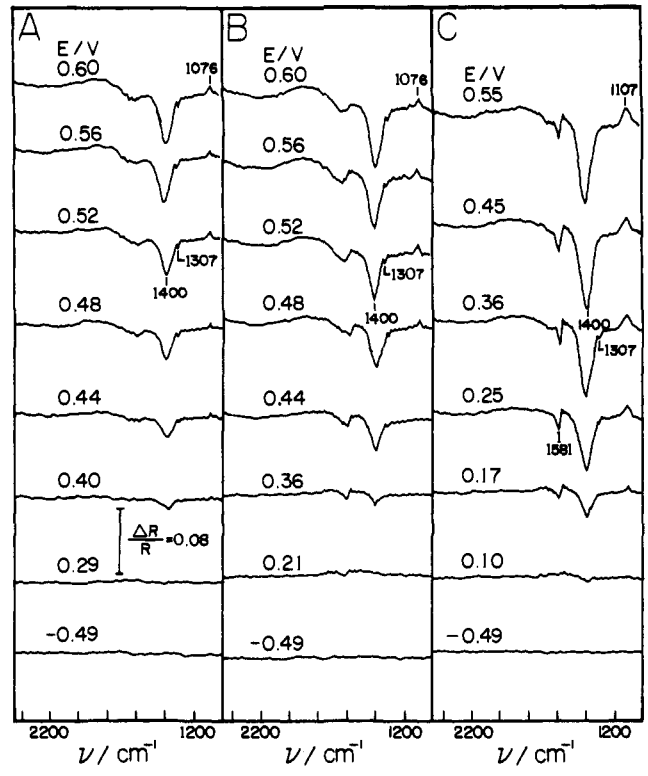

Figure 6. SPAIR spectra obtained during the voltammetric oxidation of (A) 50 mM glycolate, (B) 50 mM glyoxal, and (C) 50 mM glyoxylate in 0.5 M KOH on nickel. Potential sweep rate was 2 mV s^{-1}, positive going from −0.5 V. Other details are as in Figure 2.

−0.6 V. Consequently, then, while the production of carbonate on platinum may occur via the formate species, this route cannot account for carbonate formation from the partially oxidized C_2 reactants observed on nickel.

Given the remarkable ability of nickel to electrooxidize ethylene glycol to a singular cleaved product, formate, it is of interest to ascertain if such selective dissociative electrooxidation also applies to higher polyols. Typical SPAIR spectra for the electrooxidation of three representative polyols, glycerol, *meso*-erythritol, and D-mannitol [$(CH_2OH)(CHOH)_n(CH_2OH)$, where n = 0, 2, and 4, respectively], on nickel in 0.5 M KOH are shown in Figure 7A–C. The exclusive production of formate in each case is clearly evident in these spectra (cf. Figure 2C). Remarkably, then, the oxidized nickel surface is capable of affecting the highly efficient cleavage of *each* C–C bond in the polyol chains.

One interesting difference between these polyol reactants is that the onset of electrooxidation, as discerned from the appearance of the formate bands, shifts to slightly lower potentials as the carbon chain length increases. This difference is also evident in the corresponding cyclic voltammograms shown in Figure 8. (The dashed, dotted, and solid traces refer to glycerol, erythritol, and mannitol, respectively). The voltammograms also show that the electrooxidation rates for the higher polyols also maximize at more positive potentials, ca. 0.65 V. These two pieces of evidence suggest that the catalytic electrooxidation of the C_4 and C_6 polyols occurs with greater facility at potentials where both $Ni(OH)_2$ and NiOOH are present. [Note that the dotted curve in Figure 2C refers to the reversible $Ni(OH)_2$/NiOOH electrochemistry in 0.5 M KOH alone.]

In contrast to the highly selective C–C bond cleavage to formate observed even for the higher polyols on nickel, their electrooxidation on platinum typically yields a mixture of products. For example, glycerol electrooxidation on platinum produces both C_2 and C_3 carboxylates along with carbonate.

Two other vicinal diol compounds, 2,3-butanediol and 1,2-propanediol, were also studied on nickel in order to ascertain the possible influence of methyl groups adjacent to the hydroxy carbons. The corresponding SPAIR spectra for their electroox-

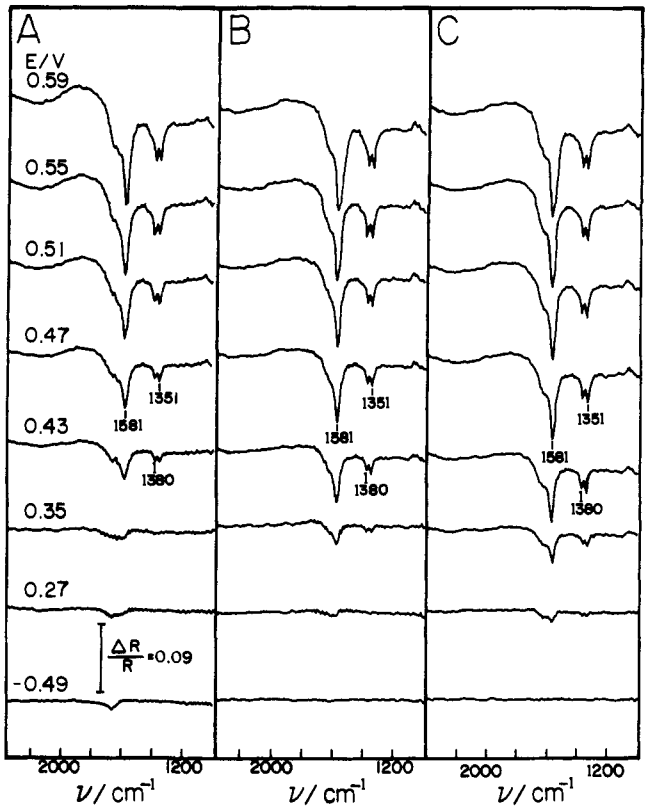

Figure 7. SPAIR spectra obtained during the voltammetric oxidation of (A) 50 mM glycerol, (B) 50 mM *meso*-erythritol, and (C) 50 mM D-mannitol in 0.5 M KOH on nickel. Potential sweep rate was 2 mV s^{-1}, positive going from −0.5 V. Other details are as in Figure 2.

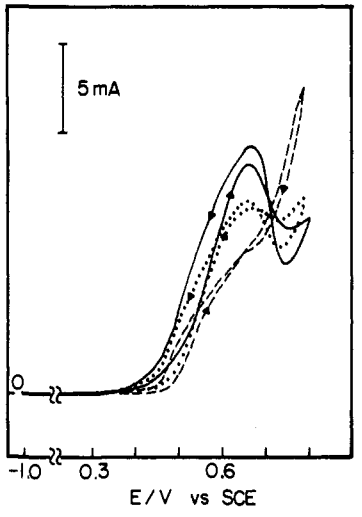

Figure 8. Cyclic voltammograms obtained at 50 mV s^{-1} for the electrooxidation of 50 mM D-mannitol (solid trace), 50 mM *meso*-erythritol (dotted trace), and 50 mM glycerol (dashed trace) in 0.5 M KOH on nickel electrode.

idation are shown in Figure 9A,B, respectively. Interestingly, these results indicate that C–C bond cleavage occurs only at the vicinal diol functionality. Thus 2,3-butanediol [$CH_3(CHOH)_2CH_3$] yields exclusively acetate (CH_3COO^-) as discerned from the appearance of the characteristic 1411/1550-cm^{-1} doublet (Figure 9A),[13] indicating that bond scission occurs only at the central, diol, position. As expected on this basis, 1,2-propanediol [$CH_3(CHOH)CH_2OH$] yields equal amounts of acetate and formate as discerned from the SPAIR spectra (Figure 9B). However, this highly selective C–C bond cleavage requires the C–OH linkages to be present on adjacent carbons, i.e., a vicinal diol. For example, electrooxidation of 1,3-propanediol yields a complex SPAIR spectrum not consistent with the equal amounts of formate and acetate anticipated

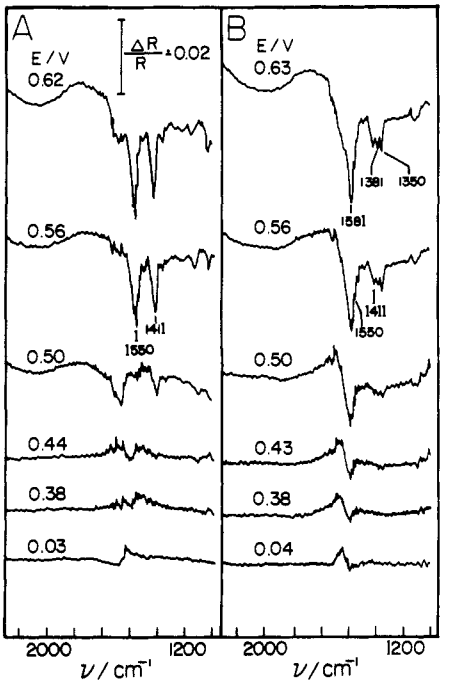

Figure 9. SPAIR spectra obtained during the voltammetric oxidation of (A) 50 mM 2,3-butanediol and (B) 50 mM 1,2-propanediol in 0.5 M KOH on nickel. Potential sweep rate was 2 mV s^{-1}, positive going from −0.5 V. Other details are as in Figure 2.

if selective C–C bond scission had occurred.

Mechanistic Implications. It is of interest to examine likely reasons for the remarkably selective electrooxidation pathways displayed by the nickel surface. The catalytic action of the nickel surface in alkaline media appears to be associated with the formation of a higher oxide, commonly termed NiOOH, from nickel hydroxide. This process appears as a reversible voltammetric wave (see dotted trace in Figure 1C). Although often formally written as a Ni(III)/(II) couple, there is evidence that the higher oxidation state approaches Ni(IV),[12] so that the redox couple can be viewed as a two-electron process.

Although the detailed interfacial chemistry responsible for the electrocatalysis is unknown, one therefore can view the nickel oxide surface couple as constituting a two-electron redox mediator. From the above results, the electrooxidation of vicinal polyols proceeds according to

$$\begin{array}{l} CH_2OH \\ | \\ (CHOH)_n \\ | \\ CH_2OH \end{array} + (n+2)[OH^-]_{Ni} \rightarrow$$

$$(n+2)HCOO^- + (2n+6)H^+ + (2n+6)e^-$$

The designation $[OH^-]_{Ni}$ refers to hydroxides, involved in oxygen transfer to the reactant, which are intimately involved in the nickel oxide film. For ethylene glycol ($n = 0$), then, a net six-electron transfer is involved, $2e^-$ of which are consumed in oxidizing the hydroxide hydrogens and $4e^-$ being used to cleave the C–C bond to yield formate. A likely molecular pathway involves binding both these carbons to adjacent oxygens on the oxidized nickel surface. This adsorbed intermediate can subsequently undergo electrooxidation by donating two electrons per carbon to the nearby nickel sites, thereby yielding a pair of formate ions. The key feature of this mechanism is the oxygen-bridged binding to a pair of nickel sites, both acting as effective two-electron oxidants. It is also possible to account for the exclusive formation of formate from the higher polyols in a similar fashion.

This mechanism for selective production of formate requires the presence of a vicinal diol functionality. Consistent with this hypothesis is the observation that glycolate, glyoxal, and glyoxalate yield primarily carbonate rather than formate. Binding of these unsymmetrical partially oxidized C_2 reactants to the nickel surface

cannot occur in the symmetric fashion available to the vicinal diols, due to the presence of at least one aldehyde or carboxylate group. One can envisage electrooxidation of such unsymmetrical reactants involving surface bonding of only one functional group.

It is interesting to compare the selective electrocatalytic properties of nickel with platinum. While the latter catalyst provides an efficient exhaustive electrooxidation of ethylene glycol and glycerol (i.e., yielding carbonate), it lacks the high degree of selectivity displayed by nickel in that comparable amounts of the exhaustive C_2 oxidation product, oxalate, are commonly formed (Figure 5). A further difference is that nickel yields selectively the *partial* oxidation product, formate. Comparison of the product distributions for electrooxidation of glycolate, glyoxal, and glyoxylate also highlights a higher efficiency of C–C bond cleavage exhibited by nickel in comparison with platinum but in somewhat different fashion. Thus electrooxidation of these C_2 species on nickel yields chiefly carbonate, with little or no oxalate formed alongside, whereas the opposite product distribution is observed on platinum.

This greater ability of the nickel surface to incur oxidative C–C bond cleavage may arise from the electropositive nature of the nickel sites and the consequent withdrawal of electron density from the carbon atoms. Whereas the nickel surface consists of a thick oxide film, the platinum surface is largely unoxidized in the potential region, −0.6 to −0.2 V, where the organic oxidative chemistry of concern here is occurring. [The latter circumstance can readily be deduced by inspecting the cyclic voltammogram (dotted curve) for Pt in 0.5 M KOH alone in Figure 1B.] Such reduced Pt surface sites can readily cleave C–H bonds, forming adsorbed hydrogen atoms, thereby providing electrooxidative pathways where the C_2 moiety remains at least partly intact, as in the production of oxalate. This property of platinum surfaces is also reflected in the facile electrooxidation of formate ($HCOO^-$) to carbonate on this metal, a process which does not occur on nickel and gold.

The present findings provide clear evidence of the virtues of real-time infrared spectroscopy for deducing in quantitative fashion detailed reaction pathways for electrocatalytic organic processes. Some marked, and in some respects unexpected, differences in the nature of the catalytic pathways for ethylene glycol electrooxidation on gold, platinum, and nickel surfaces are uncovered by these results. While gold provides pathways featuring sequential partially oxidized solution-phase intermediates, both platinum and nickel yield highly oxidized solution-phase products that are much more specific to the initial reactant. The remarkable ability of the nickel surface to incur highly selective C–C bond cleavage is intriguing and deserves future attention. Further studies of organic electrocatalysis utilizing real-time infrared spectroscopy, emphasizing ordered monocrystalline surfaces, are currently being pursued in our laboratory.

Acknowledgment. This work is supported by the National Science Foundation and the Office of Naval Research.

Registry No. $HO(CH_2)_2OH$, 107-21-1; Au, 7440-57-5; Pt, 7440-06-4; Ni, 7440-02-0; CO_3^{2-}, 3812-32-6; HCO_2^-, 71-47-6; $H_3CCO_2^-$, 71-50-1; OHCCHO, 107-22-2; $HOCH_2CO_2^-$, 57122-18-6; $HC(O)CO_2^-$, 430-75-1; $^-O_2CCO_2^-$, 338-70-5; KOH, 1310-58-3; $H_3CCH(OH)CH(OH)CH_3$, 513-85-9; $H_3CCH(OH)CH_2OH$, 57-55-6.

Characterization of the Ligand Environment of Vanadyl Complexes of Apoferritin by Multifrequency Electron Spin-Echo Envelope Modulation

Gary J. Gerfen,[†,‡] Phillip M. Hanna,[§,⊥] N. Dennis Chasteen,*[,§] and David J. Singel*[,†]

Contribution from the Departments of Chemistry, Harvard University, Cambridge, Massachusetts 02138, and University of New Hampshire, Durham, New Hampshire 03824. *Received February 6, 1991*

Abstract: The nature of the Fe^{2+} and Fe^{3+} binding sites on the protein shell of ferritin and their role in the accumulation of iron within this storage protein are poorly understood. An ESEEM (electron spin-echo envelope modulation) study is reported which provides new insight into the nature of these sites in the horse spleen protein. ESEEM spectra have been obtained of complexes of horse spleen apoferritin with VO^{2+}—an ion that binds apoferritin competitively with both Fe^{2+} and Fe^{3+}; samples prepared both in ^1H_2O and ^2H_2O and at both pH ~5.5 and at ~7.4, which correspond respectively to the α and β species of Chasteen and Theil (*J. Biol. Chem.* **1982**, *257*, 7672–7677), have been studied. The ESEEM spectra clearly reveal the presence of endogenous nitrogen in the environment of VO^{2+} in both types of complexes. This nitrogen most likely derives from an imidazole ligand of a histidine residue coordinated cis to the vanadyl oxo group. ESEEM is also observed from a proton whose dipolar coupling to the VO^{2+} center is characteristic of a hydrogen attached to the coordinated atom of a cis ligand. This hydrogen undergoes exchange with aqueous solvent; the VO^{2+} binding site is thus solvent-accessible. The ratio of the amplitude of the ESEEM peak associated with this proton in the β vs the α complex is approximately 0.5. Attribution of these ESEEM features to the hydrogens of a cis-coordinated aquo ligand that deprotonates to hydroxide at pH ≈6.5 is consistent with these observations. The ESEEM results are best interpreted in terms of a binding site that accommodates VO^{2+} with one aquo and one histidine ligand—and with other coordination positions filled by protein carboxylate donors. The possible location of this VO^{2+} binding site and its significance to iron accumulation in ferritin are discussed.

I. Introduction

Ferritins are proteins that store iron as a hydrous ferric oxide mineral core of ~80-Å diameter within a highly symmetrical assembly of 24 ~20-kDa subunit proteins.[1] In recent years, numerous studies have been undertaken to develop an understanding of the detailed process through which this storage takes place—in particular to elucidate the role played by the protein coat in the sequestration and oxidation of ferrous iron, the hy-

[†] Harvard University.
[‡] Present address: Francis Bitter National Magnet Laboratory, Massachusetts Institute of Technology, Cambridge, MA 02139.
[§] University of New Hampshire.
[⊥] Present address: National Institute of Environmental Health Sciences, P.O. Box 12233, Research Triangle Park, NC 27709.

(1) (a) Crichton, R. R. *Struct. Bonding* **1973**, *17*, 66. (b) Bourne, P. E.; Harrison, P. M.; Lewis, W. G.; Rice, D. W.; Smith, J. M. A.; Stansfield, R. F. D. In *The Biochemistry and Physiology of Iron*; Saltman, P., Heganauer, J., Eds.; Elsevier/North-Holland Biomedical: Amsterdam, 1982; p 345. (c) Crichton, R. R.; Charloteaux-Wauters, M. *Eur. J. Bioch.* **1987**, *164*, 485. (d) Theil, E. C. *Annu. Rev. Biochem.* **1987**, *56*, 289. (e) Theil, E. C. *Adv. Enzymol. Relat. Areas Mol. Biol.* **1989**, *63*, 421.

0002-7863/91/1513-9513$02.50/0